Prof. Yu Huang
State Key Lab of Loess and Quaternary Geology
Institute of Earth Environment, Chinese Academy of Sciences, Xi'an, 710061, China
Tel./Fax: (86) 29-62336261
E-mail: huangyu@ieecas.cn

Aug. 25, 2022

Dear Prof. Kourtchev,

Revision for Manuscript ACP-2022-376

We thank you very much for giving us the opportunity to revise our manuscript. We highly appreciate the reviewers for their comments and suggestions on the manuscript entitled "**Oligomer formation from the gas-phase reactions of Criegee intermediates with hydroperoxide esters: mechanism and kinetics**". We have made revisions of our manuscript carefully according to the comments and suggestions of reviewers. The revised contents are marked in blue color. The response letter to reviewers is attached at the end of this cover letter.

We hope that the revised manuscript can meet the requirement of Atmospheric Chemistry & Physics. Any further modifications or revisions, please do not hesitate to contact us.

Look forward to hearing from you as soon as possible.

Best regards,

Yu Huang

Comments of reviewer #2

1. However, a deeper discussion is required for the data in this paper. For example, in lines 263-266 "At room temperature, k_{tot} is estimated to be 3.6×10^{-10} cm^3 $molecule^{-1}$ s^{-1}, which is greater by a factor of ~3 than that reported by Welz et al. (2014) ([1.1 ± 0.1] × 10-10 cm^3 $molecule^{-1}$ s^{-1}), Chung et al. (2019) ([1.4 ± 0.3] × 10^{-10} cm^3 $molecule^{-1}$ s^{-1}), and Peltola et al. (2020) ([1.0 ± 0.03] × 10^{-10} cm^3 $molecule^{-1}$ s^{-1})". What is the reason for the difference of the k value about three times?

Response: In the original manuscript, the rate coefficients for the barrierless reactions are calculated by employing the variational transition state theory (VTST), and the rate coefficients for the bimolecular reactions with the tight transition states are computed by using the canonical transition state theory (CTST) along with one-dimensional asymmetric Eckart tunneling correction. For the initiation reactions of distinct stabilized Criegee intermediates (SCIs) with HCOOH, there are four possible pathways, namely (1) 1,4 O-H insertion (Entry 1), (2) 1,2 O-H insertion (Entry 2), (3) C-H insertion (Entry 3), and (4) C=O cycloaddition (Entry 4), in which Entry 1 is barrierless and Entry 2-4 have the tight transition states. The total rate coefficient for the reaction of SCIs with HCOOH is equal to the sum of the rate coefficient of each pathway. For the barrierless 1,4 O-H insertion reaction, the VTST is approximated with a Morse potential function, $V(R) = D_e\{1-\exp[-\beta(R-R_e)]\}^2$, along with an anisotropy potential function to stand for the minimum energy path, which is used to calculate the rate coefficients (Raghunath et al., 2017). Here, D_e is the bond energy excluding the zero-point energy, R is the reaction coordinate, and R_e is the equilibrium value of R. It is assumed that the stretching potential in an anisotropy potential is used in conjunction with a potential form of $V_{anisotropy} = V_0[1-\cos^2(\theta_1-\theta_{1e}) \times \cos^2(\theta_2-\theta_{2e})]$ (Raghunath et al., 2017). Here, V_0 is the stretching potential, which stands for by a Morse potential, θ_1 and θ_{1e} represent the rotational angle between fragment 1 and the reference axis and the equilibrium bond angle of fragment 1, θ_2 and θ_{2e} stand for the rotational angle between fragment 2 and the reference axis and the equilibrium bond angle of fragment 2. The association curve for the reaction of 1,4 O-H insertion of SCIs into HCOOH is computed at the M06-2X/6-311+G(2df,2p) level of theory to cover a range from 0.97 to 1.97 Å at step size 0.1 Å for O-H bond and from 1.44 to 2.44 Å at step size 0.1 Å for C-O bond, while other structural parameters are fully optimized. The computed potential energies are fitted to the Morse potential function. However, the calculated rate coefficients for the reactions of SCIs with HCOOH are higher than the prior experimental measurements. The reason is ascribed to the fact

that the approximation of VTST using a Morse potential function in conjunction with an anisotropy potential function is unsuitable to predict the rate coefficients for the barrierless 1,4 O-H insertion reaction.

In the revised manuscript, the rate coefficients for the barrierless reactions are computed by employing the inverse Laplace transformation (ILT) method, and the rate coefficients for the bimolecular reactions with the tight transition states are calculated by utilizing CTST in conjunction with Eckart tunneling correction. The ILT and CTST/Eckart calculations are performed by using the MESMER 6.0 and KiSThelP 2019 programs, respectively (Glowacki et al., 2012; Canneaux et al., 2013). In the ILT treatment, the rotational constants, vibrational frequencies, molecular weights, energies and other input parameters are obtained from the M06-2X/6-311+G(2df,2p) or M06-2X/ma-TZVP methods. For the barrierless reaction of 1,4 O-H insertion of SCIs into HCOOH, SCIs and HCOOH are assigned as the deficient and excess reactants, respectively. The concentration of HCOOH is given a value of 5.0×10^{10} molecules cm^{-3} in the simulation, which is taken from the typical concentration of HCOOH in the tropical forest environments (Vereecken, 2012). N_2 is applied as the buffer gas. A single exponential down model is employed to simulate the collision transfer ($<\Delta E>_{down}$ = 200 cm^{-1}). The collisional Lennard-Jones parameters are estimated with the empirical formula described by Gilbert and Smith (1990).

The rate coefficients of each elementary pathway included in the initiation reactions of distinct SCIs with HCOOH are calculated in the temperature range of 273-400 K, as listed in Table S3-S6. As shown in Table S3, the total rate coefficients $k_{tot\text{-}CH2OO}$ of CH_2OO reaction with HCOOH are in excess of 1.0×10^{-10} cm^3 $molecule^{-1}$ s^{-1}, and they exhibit a slightly negative temperature dependence in the temperature range studied. $k_{tot\text{-}CH2OO}$ is estimated to be 1.4×10^{-10} cm^3 $molecule^{-1}$ s^{-1} at 298 K, which is in good agreement with the experimental values reported by Welz et al. (2014) ($[1.1 \pm 0.1] \times 10^{-10}$), Chung et al. (2019) ($[1.4 \pm 0.3] \times 10^{-10}$), and Peltola et al. (2020) ($[1.0 \pm 0.03] \times 10^{-10}$). $k(TS_{ent1})$ is approximately equal to $k_{tot\text{-}CH2OO}$ in the whole temperature range, and it decreases in the range of 1.7×10^{-10} (273 K) to 1.2×10^{-10} (400 K) cm^3 $molecule^{-1}$ s^{-1} with increasing temperature. $k(TS_{ent1})$ is several orders of magnitude greater than $k(TS_{ent2})$, $k(TS_{ent3})$ and $k(TS_{ent4})$ over the temperature range from 273 to 400 K. The result again shows that the barrierless 1,4 O-H insertion reaction is predominant. Similar conclusion is also obtained from the results of the rate coefficients for the reactions of HCOOH with *anti*-CH_3CHOO, *syn*-CH_3CHOO and $(CH_3)_2COO$ (Table S4-S6).

At ambient temperature, the total rate coefficients of HCOOH reactions with *anti*-CH_3CHOO, *syn*-CH_3CHOO and $(CH_3)_2COO$ are estimated to be 5.9, 2.7 and 4.8 × 10^{-10} cm^3 $molecule^{-1}$ s^{-1}, respectively, which are consistent with the prior experimental measurements of 5 ± 3, 2.5 ± 0.3 and 4.5 × 10^{-10} cm^3 $molecule^{-1}$ s^{-1} (Welz et al., 2014; Chung et al., 2019; Sipilä et al., 2014).

Table S3 Rate coefficients (cm^3 $molecule^{-1}$ s^{-1}) of each elementary pathway involved in the initiation reaction of CH_2OO with HCOOH computed at different temperatures

T/K	k (TS_{ent1})	k (TS_{ent2})	k (TS_{ent3})	k (TS_{ent4})	$k_{tot\text{-}CH2OO}$
273	1.7×10^{-10}	3.6×10^{-12}	1.0×10^{-22}	3.6×10^{-12}	1.8×10^{-10}
280	1.6×10^{-10}	2.9×10^{-12}	1.2×10^{-22}	3.1×10^{-12}	1.7×10^{-10}
298	1.4×10^{-10}	1.9×10^{-12}	2.2×10^{-22}	2.3×10^{-12}	1.4×10^{-10}
300	1.4×10^{-10}	1.8×10^{-12}	2.4×10^{-22}	2.2×10^{-12}	1.4×10^{-10}
320	1.3×10^{-10}	1.2×10^{-12}	4.9×10^{-22}	1.6×10^{-12}	1.3×10^{-10}
340	1.3×10^{-10}	8.2×10^{-13}	1.0×10^{-21}	1.3×10^{-12}	1.3×10^{-10}
360	1.2×10^{-10}	5.9×10^{-13}	2.2×10^{-21}	1.0×10^{-12}	1.2×10^{-10}
380	1.2×10^{-10}	4.5×10^{-13}	4.5×10^{-21}	8.2×10^{-13}	1.2×10^{-10}
400	1.2×10^{-10}	3.5×10^{-13}	9.0×10^{-21}	6.9×10^{-13}	1.2×10^{-10}

Table S4 Rate coefficients (cm^3 $molecule^{-1}$ s^{-1}) of each elementary pathway involved in the initiation reaction of *anti*-CH_3CHOO with HCOOH computed at different temperatures

T/K	k (TS_{ent1}-*anti*)	k (TS_{ent2}-*anti*)	k (TS_{ent3}-*anti*)	k (TS_{ent4}-*anti*)	$k_{tot\text{-}anti}$
273	5.9×10^{-10}	4.2×10^{-11}	5.5×10^{-22}	6.1×10^{-11}	6.9×10^{-10}
280	5.7×10^{-10}	3.8×10^{-11}	6.7×10^{-22}	4.9×10^{-11}	6.6×10^{-10}
298	5.4×10^{-10}	2.3×10^{-11}	1.2×10^{-21}	3.0×10^{-11}	5.9×10^{-10}
300	5.3×10^{-10}	2.0×10^{-11}	1.3×10^{-21}	2.8×10^{-11}	5.8×10^{-10}
320	5.0×10^{-10}	1.5×10^{-11}	2.6×10^{-21}	1.7×10^{-11}	5.3×10^{-10}
340	4.7×10^{-10}	9.4×10^{-12}	5.4×10^{-21}	1.1×10^{-11}	4.9×10^{-10}
360	4.5×10^{-10}	7.0×10^{-12}	1.1×10^{-20}	7.8×10^{-12}	4.7×10^{-10}
380	4.4×10^{-10}	3.6×10^{-12}	2.1×10^{-20}	5.6×10^{-12}	4.5×10^{-10}
400	4.3×10^{-10}	2.0×10^{-12}	4.0×10^{-20}	4.2×10^{-12}	4.4×10^{-10}

Table S5 Rate coefficients (cm^3 $molecule^{-1}$ s^{-1}) of each elementary pathway involved in the initiation reaction of *syn*-CH_3CHOO with HCOOH computed at different temperatures

T/K	k (TS_{ent1}-*syn*)	k (TS_{ent2}-*syn*)	k (TS_{ent3}-*syn*)	k (TS_{ent4}-*syn*)	$k_{tot\text{-}syn}$
273	3.1×10^{-10}	9.5×10^{-13}	4.6×10^{-27}	7.5×10^{-16}	3.1×10^{-10}
280	2.8×10^{-10}	8.0×10^{-13}	7.1×10^{-27}	6.4×10^{-16}	2.8×10^{-10}
298	2.7×10^{-10}	5.4×10^{-13}	8.9×10^{-26}	5.5×10^{-16}	2.7×10^{-10}
300	2.7×10^{-10}	5.2×10^{-13}	9.9×10^{-26}	4.6×10^{-16}	2.7×10^{-10}
320	2.5×10^{-10}	3.6×10^{-13}	3.0×10^{-25}	3.8×10^{-16}	2.5×10^{-10}
340	2.5×10^{-10}	2.6×10^{-13}	9.1×10^{-25}	3.1×10^{-16}	2.5×10^{-10}
360	2.3×10^{-10}	2.0×10^{-13}	2.6×10^{-24}	3.0×10^{-16}	2.3×10^{-10}
380	2.2×10^{-10}	1.5×10^{-13}	7.2×10^{-24}	2.4×10^{-16}	2.2×10^{-10}
400	2.2×10^{-10}	1.2×10^{-13}	1.8×10^{-23}	2.2×10^{-16}	2.2×10^{-10}

Table S6 Rate coefficients (cm^3 $molecule^{-1}$ s^{-1}) of each elementary pathway involved in the initiation reaction of $(CH_3)_2OO$ with HCOOH computed at different temperatures

T/K	k (TS_{ent1}-*dim*)	k (TS_{ent2}-*dim*)	k (TS_{ent3}-*dim*)	k (TS_{ent4}-*dim*)	$k_{tot\text{-}dim}$
273	5.3×10^{-10}	6.8×10^{-12}	1.4×10^{-26}	4.4×10^{-15}	5.4×10^{-10}
280	5.1×10^{-10}	5.2×10^{-12}	2.2×10^{-26}	4.2×10^{-15}	5.2×10^{-10}
298	4.8×10^{-10}	2.8×10^{-12}	8.0×10^{-26}	4.0×10^{-15}	4.8×10^{-10}
300	4.7×10^{-10}	2.6×10^{-12}	9.2×10^{-26}	3.9×10^{-15}	4.7×10^{-10}
320	4.5×10^{-10}	1.4×10^{-12}	3.6×10^{-25}	3.7×10^{-15}	4.5×10^{-10}
340	4.2×10^{-10}	8.6×10^{-13}	1.3×10^{-24}	3.6×10^{-15}	4.2×10^{-10}
360	3.9×10^{-10}	5.5×10^{-13}	4.5×10^{-24}	3.5×10^{-15}	3.9×10^{-10}
380	3.7×10^{-10}	3.7×10^{-13}	1.4×10^{-23}	3.4×10^{-15}	3.7×10^{-10}
400	3.7×10^{-10}	2.6×10^{-13}	3.9×10^{-23}	3.4×10^{-15}	3.7×10^{-10}

Corresponding descriptions have been added in the page 7 line 173-190, page 11 line 303-315, page 12 line 330-338 and page 13 line 346-351 of the revised manuscript:

The rate coefficients for the barrierless reactions are determined by employing the inverse Laplace transformation (ILT) method. The ILT calculations are performed with the MESMER 6.0 program (Glowacki et al., 2012). In the ILT treatment, the rotational constants, vibrational frequencies, molecular weights, energies and other input parameters are obtained from the M06-2X/6-311+G(2df,2p) or M06-2X/ma-TZVP methods. For the barrierless reaction of 1,4 O-H

insertion of SCIs into HCOOH, SCIs and HCOOH are assigned as the deficient and excess reactants, respectively. The concentration of HCOOH is given a value of 5.0 × 10^{10} molecules cm^{-3} in the simulation, which is taken from the typical concentration of HCOOH in the tropical forest environments (Vereecken et al., 2012). N_2 is applied as the buffer gas. A single exponential down model is employed to simulate the collision transfer ($\langle\Delta E\rangle_{down}$ = 200 cm^{-1}). The collisional Lennard-Jones parameters are estimated with the empirical formula described by Gilbert and Smith (1990).

The rate coefficients for the bimolecular reactions with the tight transition states are calculated by using the canonical transition state theory (CTST) along with one-dimensional asymmetric Eckart tunneling correction (Truhlar et al., 1996; Eckart, 1930). The CTST/Eckart calculations are performed with the KiSThelP 2019 program (Canneaux et al., 2013).

The rate coefficients of each elementary pathway included in the initiation reactions of distinct SCIs with HCOOH are calculated in the temperature range of 273-400 K, as listed in Table S3-S6. As shown in Table S3, the total rate coefficients $k_{tot\text{-}CH2OO}$ of CH_2OO reaction with HCOOH are in excess of 1.0 × 10^{-10} cm^3 $molecule^{-1}$ s^{-1}, and they exhibit a slightly negative temperature dependence in the temperature range studied. $k_{tot\text{-}CH2OO}$ is estimated to be 1.4 × 10^{-10} cm^3 $molecule^{-1}$ s^{-1} at 298 K, which is in good agreement with the experimental values reported by Welz et al. (2014) ([1.1 ± 0.1] × 10^{-10}), Chung et al. (2019) ([1.4 ± 0.3] × 10^{-10}), and Peltola et al. (2020) ([1.0 ± 0.03] × 10^{-10}). $k(TS_{ent1})$ is approximately equal to $k_{tot\text{-}CH2OO}$ in the whole temperature range, and it decreases in the range of 1.7 × 10^{-10} (273 K) to 1.2 × 10^{-10} (400 K) cm^3 $molecule^{-1}$ s^{-1} with increasing temperature. $k(TS_{ent1})$ is several orders of magnitude greater than $k(TS_{ent2})$, $k(TS_{ent3})$ and $k(TS_{ent4})$ over the temperature range from 273 to 400 K. The result again shows that the barrierless 1,4 O-H insertion reaction is predominant.

Equivalent to the case of CH_2OO reaction with HCOOH, the rate coefficient of each elementary pathway involved in the anti-CH_3CHOO + HCOOH reaction also decreases with the temperature increasing (Table S4). This table shows that Entry 1 is kinetically favored over Entry 2, 3 and 4, and Entry 2 is competitive with Entry 4 in the range 273-400 K. Similar conclusion is also obtained from the results of the rate coefficients for the reactions of syn-CH_3CHOO and $(CH_3)_2COO$ with HCOOH that Entry 1 is the dominant pathway (Table S5-S6). It deserves mentioning that the competition of Entry 2 is significantly greater than that of Entry 4 in the syn-

CH_3CHOO + HCOOH and $(CH_3)_2COO$ + HCOOH systems. At ambient temperature, the total rate coefficients of HCOOH reactions with anti-CH_3CHOO, syn-CH_3CHOO and $(CH_3)_2COO$ are estimated to be 5.9, 2.7 and 4.8 × 10^{-10} cm^3 $molecule^{-1}$ s^{-1}, respectively, which are consistent with the prior experimental measurements of 5 ± 3, 2.5 ± 0.3 and 4.5 × 10^{-10} cm^3 $molecule^{-1}$ s^{-1} (Welz et al., 2014; Chung et al., 2019; Sipilä et al., 2014).

2. Furthermore, this paper should also exhibit some extended discussions about atmospheric implications of these reactions and their products. For example, what is the role of the formed oligomers on the atmosphere? It follows in the requirements of ACP journal "The journal scope is focused on studies with important implications for our understanding of the state and behavior of the atmosphere. Articles with a local focus must clearly explain how the results extend and compare with current knowledge".

Response: Based on the Reviewer's suggestion, the atmospheric implication of the reactions of SCIs with hydroperoxide esters and the role of the formed oligomers have been added in the revised manuscript. It is well known that the reactions with trace species (e.g., H_2O, HCOOH and SO_2) are expected to be the dominant chemical sinks for SCIs in the atmosphere (Taatjes et al., 2013; Long et al., 2016). The relative importance of distinct SCIs reactions with hydroperoxide esters and trace species is taken into account. In the present study, the hydroperoxymethyl formate (HPMF) is selected as the model compound since it is the simplest hydroperoxide ester formed from the barrierless reaction of 1,4 O-H insertion of CH_2OO into HCOOH. The reported concentrations of coreactant, the rate coefficients k, and the effective pseudo-first-order rate constants (k_{eff} = k[coreactant]) for distinct SCI reactions with H_2O, HCOOH, SO_2, and HPMF are summarized in Table 2. As seen in Table 2, the rate coefficient of a particular SCI reaction with trace species is strongly dependent on its structure. The methyl group substitution may alter the rate coefficient by several to tens of times. The atmospheric concentrations of H_2O, HCOOH and SO_2 in the tropical forest environments are measured to be 3.9-6.1 × 10^{17}, 5.0-10 × 10^{10}, and 1.7-9.0 × 10^{10} molecules cm^{-3}, respectively (Vereecken, 2012). For the reactions of CH_2OO with H_2O, HCOOH, and SO_2, the experimental rate coefficients are determined to be < 1.5 × 10^{-15}, [1.1 ± 0.1] × 10^{-10}, and [3.9 ± 0.7] × 10^{-11} cm^3 $molecule^{-1}$ s^{-1}, respectively (Welz et al., 2012 and 2014; Chao et al., 2015), which translate into $k_{eff(CH2OO+H2O)}$, $k_{eff(CH2OO+HCOOH)}$ and $k_{eff(CH2OO+SO2)}$ of 5.9-9.2 × 10^2, 5.5-11, and 0.7-

3.5 s^{-1}, respectively. The result reveals that the reaction of CH_2OO with H_2O is the most important bimolecular reaction. $k_{eff(CH2OO+HCOOH)}$ is greater by a factor of 3-8 than $k_{eff(CH2OO+SO2)}$, indicating that the reaction of CH_2OO with HCOOH is favored over reaction with SO_2. Similar conclusion is also obtained from the results of k_{eff} for the reactions of *anti*-CH_3CHOO, *syn*-CH_3CHOO and $(CH_3)_2COO$ with H_2O, HCOOH and SO_2 that SCIs reactions with H_2O are faster than with HCOOH, which, in turn, are faster than with SO_2.

According to the results shown in the Table 2, the room temperature rate coefficient for the reaction of CH_2OO with HPMF is calculated to be 2.7×10^{-11} cm^3 $molecule^{-1}$ s^{-1}. However, to the best of our knowledge, the atmospheric concentration of HPMF has not been reported up to now. If we assume that the concentration of HPMF is the same as that of HCOOH, $k_{eff(CH2OO+HPMF)}$ is estimated to be 1.4-2.7 s^{-1}, which is significantly lower than $k_{eff(CH2OO+H2O)}$ and $k_{eff(CH2OO+HCOOH)}$. $k_{eff(CH2OO+HPMF)}$ is nearly identical to $k_{eff(CH2OO+SO2)}$, indicating that the CH_2OO + HPMF reaction is competitive with the CH_2OO + SO_2 system. Previous model-measurement studies have estimated the surface-level SCIs concentrations in the range of 1.0×10^4 to 1.0×10^5 molecules cm^{-3} (Khan et al., 2018; Novelli et al., 2017). If we assume that the concentration of HPMF is equal to that of SCIs, $k_{eff(CH2OO+HPMF)}$ is calculated to be 2.7-27 $\times 10^{-7}$ s^{-1}, which is several orders of magnitude lower than $k_{eff(CH2OO+H2O)}$, $k_{eff(CH2OO+HCOOH)}$ and $k_{eff(CH2OO+SO2)}$. This result indicates that the reaction of CH_2OO with HPMF is of less importance. Similar conclusion is also obtained from the reactions of *anti*-CH_3CHOO, *syn*-CH_3CHOO and $(CH_3)_2COO$ with HPMF. Based on the above discussions, it can be concluded that the relative importance of carbonyl oxides reactions with hydroperoxide esters is significantly dependent on the concentrations of hydroperoxide esters. These reactions may play a certain role in the formation of organic new particle in some regions where low concentration of water vapour and high concentration of hydroperoxide esters occur.

The vapour pressure and volatility of the formed oligomers are estimated in the revised manuscript. The assessment of Barley and McFiggans (2010) and O'Meara et al. (2014) found that the combination of boiling point estimation from Nannoolal et al. (2004) and vapour pressure estimation from Nannoolal et al. (2008) gives the lowest mean bias error of vapour pressure for atmospherically relevant compounds. Therefore, the saturated vapour pressure (P^0) of adduct products at room temperature is estimated by using the Nannoolal-Nannoolal method, and the results are listed in Table S10. From Table S10, it can be seen that the P^0 of adduct products involved

in the successive reactions of CH_2OO with HCOOH increases first and then decreases with increasing the number of CH_2OO. The P^0 of the adduct product $HC(O)O(CH_2OO)_3H$ is maximum when the number of CH_2OO is equal to three. The P^0 of adduct products included in the successive reactions of *anti*-CH_3CHOO with HCOOH decreases significantly as the number of *anti*-CH_3CHOO is increased. Similar phenomenon is also observed from the successive reactions of *syn*-CH_3CHOO and $(CH_3)_2COO$ with HCOOH. Notably, the P^0 of adduct products decreases obviously when the size of SCIs increases. For example, the P^0 of the adduct product $HC(O)O(CH_2OO)_3H$ in the nCH_2OO + HCOOH reaction is estimated to be 4.43×10^{-3} atm, which is greater than those of the corresponding adduct products in the n*anti*-CH_3CHOO + HCOOH (7.12×10^{-4}), n*syn*-CH_3CHOO + HCOOH (7.12×10^{-4}), and n$(CH_3)_2COO$ + HCOOH (1.27×10^{-4}) reactions by 6.22, 6.22 and 34.88 times, respectively.

A classify scheme of various organic compounds is based on their volatility, as presented by Donahue et al. (2012) The volatility of organic compounds is described by their effective saturation concentration. The saturated concentrations (c^0) of adduct products formed from the successive reactions of SCIs with HCOOH are predicted with the SIMPOL.1 method proposed by Pankow and Asher (2008), and the results are listed in Table S10. As shown in Table S10, the c^0 of adduct products involved in the nCH_2OO + HCOOH reaction decreases with increasing the number of CH_2OO. According to the Volatility Basis Set (VBS) of organic compounds (Donahue et al., 2012), these adduct products belong to volatile organic compound (VOC) ($c^0 > 3 \times 10^6$ ug/m^3). Similarly, the c^0 of adduct products included in the n*anti*-CH_3CHOO + HCOOH, n*syn*-CH_3CHOO + HCOOH, and n$(CH_3)_2COO$ + HCOOH reactions decreases when the number of SCIs increases. It deserves mentioning that the adduct products in the n*anti*-CH_3CHOO + HCOOH and n*syn*-CH_3CHOO + HCOOH reactions belong to intermediate volatility organic compounds (IVOC, $300 < c^0 < 3 \times 10^6$ ug/m^3) when the number of SCIs is equal to five. However, the adduct products in the n$(CH_3)_2COO$ + HCOOH reaction become IVOC when the number of $(CH_3)_2COO$ is greater than or equal to two. Based on the above discussions, it can be concluded that the volatility of adduct products is significantly affected by the number and size of SCIs in the successive reaction of SCIs with HCOOH.

Table 2 The reported concentrations of coreactant, the rate coefficients *k*, and the effective pseudo-first-order rate constants ($k_{eff} = k$[coreactant]) for distinct SCI reactions with HPMF, H_2O, HCOOH

and SO_2 at the tropical forest environments

SCIs	Coreactant	[Coreactant] (molecules cm^{-3})	k (cm^3 $molecule^{-1}$ s^{-1})	k_{eff} (s^{-1})	Reference
CH_2OO	H_2O	$3.9\text{-}6.1 \times 10^{17}$	$< 1.5 \times 10^{-15}$	$5.9\text{-}9.2 \times 10^2$	Chao et al., (2015)
	HCOOH	$5.0\text{-}10.0 \times 10^{10}$	$[1.1 \pm 0.1] \times 10^{-10}$	5.5-11	Welz et al., (2014)
	SO_2	$1.7\text{-}9.0 \times 10^{10}$	$[3.9 \pm 0.7] \times 10^{-11}$	0.7-3.5	Welz et al., (2012)
	HPMF	-	2.7×10^{-11}	-	This work
anti-CH_3CHOO	H_2O	$3.9\text{-}6.1 \times 10^{17}$	$[1.0 \pm 0.4] \times 10^{-14}$	$3.9\text{-}6.1 \times 10^3$	Taatjes et al., (2013)
	HCOOH	$5.0\text{-}10.0 \times 10^{10}$	$[5 \pm 3] \times 10^{-10}$	25.0-50.0	Welz et al., (2014)
	SO_2	$1.7\text{-}9.0 \times 10^{10}$	$[6.7 \pm 1.0] \times 10^{-11}$	1.1-6.0	Taatjes et al., (2013)
	HPMF	-	3.3×10^{-10}	-	This work
syn-CH_3CHOO	H_2O	$3.9\text{-}6.1 \times 10^{17}$	$< 4.0 \times 10^{-15}$	$1.6\text{-}2.4 \times 10^3$	Taatjes et al., (2013)
	HCOOH	$5.0\text{-}10.0 \times 10^{10}$	$[2.5 \pm 0.3] \times 10^{-10}$	12.5-25.0	Welz et al., (2014)
	SO_2	$1.7\text{-}9.0 \times 10^{10}$	$[2.4 \pm 0.3] \times 10^{-11}$	0.4-2.2	Taatjes et al., (2013)
	HPMF	-	1.7×10^{-13}	-	This work
$(CH_3)_2COO$	H_2O	$3.9\text{-}6.1 \times 10^{17}$	$< 1.5 \times 10^{-16}$	58.5-91.5	Huang et al., (2015)
	HCOOH	$5.0\text{-}10.0 \times 10^{10}$	4.5×10^{-10}	22.5-45.0	Sipilä et al., (2014)
	SO_2	$1.7\text{-}9.0 \times 10^{10}$	1.3×10^{-10}	2.2-11.7	Huang et al., (2015)
	HPMF	-	2.2×10^{-11}	-	This work

Table S10 Predicted saturated vapour pressure (P^0) and saturated concentrations (c^0) for the adduct products of the successive reactions of SCIs with HCOOH

	formula	P^0 (atm)	c^0 (ug/m^3)
n CH_2OO + HCOOH			
n = 1	$HC(O)OCH_2OOH$	2.12×10^{-3}	7.86×10^7
n = 2	$HC(O)O(CH_2OO)_2H$	3.80×10^{-3}	3.99×10^7
n = 3	$HC(O)O(CH_2OO)_3H$	4.43×10^{-3}	3.91×10^7

n = 4	$HC(O)O(CH_2OO)_4H$	4.21×10^{-3}	3.29×10^{7}
n = 5	$HC(O)O(CH_2OO)_5H$	3.59×10^{-3}	2.12×10^{7}
n *anti*-CH_3CHOO + HCOOH			
n = 1	$HC(O)OCH(CH_3)OOH$	1.25×10^{-3}	8.32×10^{6}
n = 2	$HC(O)O(CH(CH_3)OO)_2H$	1.13×10^{-3}	7.57×10^{6}
n = 3	$HC(O)O(CH(CH_3)OO)_3H$	7.12×10^{-4}	6.49×10^{6}
n = 4	$HC(O)O(CH(CH_3)OO)_4H$	3.90×10^{-4}	4.50×10^{6}
n = 5	$HC(O)O(CH(CH_3)OO)_5H$	2.01×10^{-4}	2.81×10^{6}
n *syn*-CH_3CHOO + HCOOH			
n = 1	$HC(O)OCH(CH_3)OOH$	1.25×10^{-3}	8.32×10^{6}
n = 2	$HC(O)O(CH(CH_3)OO)_2H$	1.13×10^{-3}	7.57×10^{6}
n = 3	$HC(O)O(CH(CH_3)OO)_3H$	7.12×10^{-4}	6.49×10^{6}
n = 4	$HC(O)O(CH(CH_3)OO)_4H$	3.90×10^{-4}	4.50×10^{6}
n = 5	$HC(O)O(CH(CH_3)OO)_5H$	2.01×10^{-4}	2.81×10^{6}
n $(CH_3)_2COO$ + HCOOH			
n = 1	$HC(O)OC(CH_3)_2OOH$	7.23×10^{-4}	3.50×10^{6}
n = 2	$HC(O)O(C(CH_3)_2OO)_2H$	3.50×10^{-4}	2.74×10^{6}
n = 3	$HC(O)O(C(CH_3)_2OO)_3H$	1.27×10^{-4}	1.38×10^{6}
n = 4	$HC(O)O(C(CH_3)_2OO)_4H$	4.27×10^{-5}	5.90×10^{5}
n = 5	$HC(O)O(C(CH_3)_2OO)_5H$	1.40×10^{-5}	2.36×10^{5}

Corresponding descriptions have been added in the page 23 line 573-590, page 24 line 591-610, page 27 line 645-671 and page 28 line 672-682 of the revised manuscript:

It is of interest to assess whether the reactions of distinct SCIs with HPMF can compete well with the losses to reactions with trace species (e.g., H_2O, HCOOH and SO_2), because it is well known that the reactions with trace species are expected to be the dominant chemical sinks for SCIs in the atmosphere (Taatjes et al., 2013; Long et al., 2016). The reported concentrations of coreactant, the rate coefficients k, and the effective pseudo-first-order rate constants (k_{eff} = k[coreactant]) for distinct SCI reactions with H_2O, HCOOH, SO_2, and HPMF are summarized in Table 2. As seen in Table 2, the rate coefficient of a particular SCI reaction with trace species is strongly dependent on its structure. The methyl group substitution may alter the rate coefficient by several to tens of times. The atmospheric concentrations of H_2O, HCOOH and SO_2 in the tropical forest environments are measured to be 3.9-6.1 $\times 10^{17}$, 5.0-10 $\times 10^{10}$, and 1.7-9.0 $\times 10^{10}$ molecules cm^{-3}, respectively (Vereecken, 2012). For the reactions of CH_2OO with H_2O, HCOOH, and SO_2, the experimental rate coefficients are determined to be $< 1.5 \times 10^{-15}$, $[1.1 \pm 0.1] \times 10^{-10}$, and $[3.9 \pm 0.7] \times 10^{-11}$ cm^3 $molecule^{-1}$ s^{-1}, respectively (Welz et al., 2012 and 2014; Chao et al., 2015), which translate into

$k_{eff(CH2OO+H2O)}$, $k_{eff(CH2OO+HCOOH)}$ and $k_{eff(CH2OO+SO2)}$ of 5.9-9.2 × 10^{2}, 5.5-11, and 0.7-3.5 s^{-1}, respectively. The result reveals that the reaction of CH_2OO with H_2O is the most important bimolecular reaction. $k_{eff(CH2OO+HCOOH)}$ is greater by a factor of 3-8 than $k_{eff(CH2OO+SO2)}$, indicating that the reaction of CH_2OO with HCOOH is favored over reaction with SO_2. Similar conclusion is also obtained from the results of k_{eff} for the reactions of anti-CH_3CHOO, syn-CH_3CHOO and $(CH_3)_2COO$ with H_2O, HCOOH and SO_2 that SCIs reactions with H_2O are faster than with HCOOH, which, in turn, are faster than with SO_2.

According to the results shown in the Table 2, the room temperature rate coefficient for the reaction of CH_2OO with HPMF is calculated to be 2.7 × 10^{-11} cm^3 $molecule^{-1}$ s^{-1}. However, to the best of our knowledge, the atmospheric concentration of HPMF has not been reported up to now. If we assume that the concentration of HPMF is the same as that of HCOOH, $k_{eff(CH2OO+HPMF)}$ is estimated to be 1.4-2.7 s^{-1}, which is significantly lower than $k_{eff(CH2OO+H2O)}$ and $k_{eff(CH2OO+HCOOH)}$. $k_{eff(CH2OO+HPMF)}$ is nearly identical to $k_{eff(CH2OO+SO2)}$, indicating that the CH_2OO + HPMF reaction is competitive with the CH_2OO + SO_2 system. Previous model-measurement studies have estimated the surface-level SCIs concentrations in the range of 1.0 × 10^{4} to 1.0 × 10^{5} molecules cm^{-3} (Khan et al., 2018; Novelli et al., 2017). If we assume that the concentration of HPMF is equal to that of SCIs, $k_{eff(CH2OO+HPMF)}$ is calculated to be 2.7-27 × 10^{-7} s^{-1}, which is several orders of magnitude lower than $k_{eff(CH2OO+H2O)}$, $k_{eff(CH2OO+HCOOH)}$ and $k_{eff(CH2OO+SO2)}$. This result indicates that the reaction of CH_2OO with HPMF is of less importance. Similar conclusion is also obtained from the reactions of anti-CH_3CHOO, syn-CH_3CHOO and $(CH_3)_2COO$ with HPMF. Based on the above discussions, it can be concluded that the relative importance of carbonyl oxides reactions with hydroperoxide esters is significantly dependent on the concentrations of hydroperoxide esters. These reactions may play a certain role in the formation of organic new particle in some regions where low concentration of water vapour and high concentration of hydroperoxide esters occur.

The assessment of Barley and McFiggans (2010) and O'Meara et al. (2014) found that the combination of boiling point estimation from Nannoolal et al. (2004) and vapour pressure estimation from Nannoolal et al. (2008) gives the lowest mean bias error of vapour pressure for atmospherically relevant compounds. Therefore, the saturated vapour pressure (P^0) of adduct products at room temperature is estimated by using the Nannoolal-Nannoolal method, and the results are listed in Table S10. From Table S10, it can be seen that the P^0 of adduct products involved

in the successive reactions of CH_2OO with HCOOH increases first and then decreases with increasing the number of CH_2OO. The P^0 of the adduct product $HC(O)O(CH_2OO)_3H$ is maximum when the number of CH_2OO is equal to three. The P^0 of adduct products included in the successive reactions of anti-CH_3CHOO with HCOOH decreases significantly as the number of anti-CH_3CHOO is increased. Similar phenomenon is also observed from the successive reactions of syn-CH_3CHOO and $(CH_3)_2COO$ with HCOOH. Notably, the P^0 of adduct products decreases obviously when the size of SCIs increases. For example, the P^0 of the adduct product $HC(O)O(CH_2OO)_3H$ in the nCH_2OO + HCOOH reaction is estimated to be 4.43×10^{-3} atm, which is greater than those of the corresponding adduct products in the nanti-CH_3CHOO + HCOOH (7.12×10^{-4}), nsyn-CH_3CHOO + HCOOH (7.12×10^{-4}), and $n(CH_3)_2COO$ + HCOOH (1.27×10^{-4}) reactions by 6.22, 6.22 and 34.88 times, respectively.

A classify scheme of various organic compounds is based on their volatility, as presented by Donahue et al. (2012) The volatility of organic compounds is described by their effective saturation concentration. The saturated concentrations (c^0) of adduct products formed from the successive reactions of SCIs with HCOOH are predicted by using the SIMPOL.1 method proposed by Pankow and Asher (2008), and the results are listed in Table S10. As shown in Table S10, the c^0 of adduct products involved in the nCH_2OO + HCOOH reaction decreases with increasing the number of CH_2OO. According to the Volatility Basis Set (VBS) of organic compounds (Donahue et al., 2012), these adduct products belong to VOC ($c^0 > 3 \times 10^6$ ug/m^3). Similarly, the c^0 of adduct products included in the nanti-CH_3CHOO + HCOOH, nsyn-CH_3CHOO + HCOOH, and $n(CH_3)_2COO$ + HCOOH reactions decreases when the number of SCIs increases. It deserves mentioning that the adduct products in the nanti-CH_3CHOO + HCOOH and nsyn-CH_3CHOO + HCOOH reactions belong to intermediate volatility organic compounds (IVOC, $300 < c^0 < 3 \times 10^6$ ug/m^3) when the number of SCIs is equal to five. However, the adduct products in the $n(CH_3)_2COO$ + HCOOH reaction become IVOC when the number of $(CH_3)_2COO$ is greater than or equal to two. Based on the above discussions, it can be concluded that the volatility of adduct products is significantly affected by the number and size of SCIs in the successive reaction of SCIs with HCOOH.

3. Hence, as a quick assessment, some deeper and extended discussions should be required and strengthened, such as the nature of the reactions, the detailed atmospheric implications, if this paper

is published in the ACP journal.

Response: Based on the Reviewer's suggestion, the deeper discussions on the nature of the reactions of SCIs with hydroperoxide esters have been added in the revised manuscript. A schematic potential energy surface (PES) for the addition reaction $2CH_2OO$ + Pent1a is drawn in Fig. 2. As seen in Fig. 2, the successive insertion of CH_2OO into Pent1a eventually leads to the formation of oligomers P2a and P2b composed of CH_2OO as the repeat unit. These oligomerization reactions are strongly exothermic and spontaneous (> 83 kcal·mol^{-1}), implying that they are feasible thermodynamically. The addition reaction $2CH_2OO$ + Pent1a initially proceeds through two possible pathways, namely (1) –OOH insertion reaction R1a, and (2) –CH insertion reaction R1b. For the –OOH insertion reaction R1a, the pre-reactive intermediate IM1a with a seven-membered ring structure is formed in the entrance channel, which is stabilized by the hydrogen bond interactions between the H_4 atom of Pent1a and the O_6 atom of CH_2OO ($D_{(O6-H4)}$ = 1.706 Å), and between the H_6 atom of CH_2OO and the O_3 atom of Pent1a ($D_{(O3-H6)}$ = 2.115 Å). Then IM1a converts into P1a ($C_3H_6O_6$, HC(O)O–$(CH_2OO)_2$–H) via a concerted process of O_4-H_4 bond breaking in the Pent1a and O_4-C_3 and H_4-O_6 bonds forming with a barrier of 8.1 kcal·mol^{-1}. For the –CH insertion reaction R1b, the pre-reactive intermediate IM1b with a seven-membered ring structure is formed in the entrance channel, which is stabilized by the van der Waals (vdW) interactions between the O_3 atom of Pent1a and the C_3 atom of CH_2OO ($D_{(O3-C3)}$ = 2.602 Å), and between the O_6 atom of CH_2OO and the C_1 atom of Pent1a ($D_{(O6-C1)}$ = 2.608 Å). Due to the absence of hydrogen bond in IM1b, the energy of IM1b is lower than that of IM1a by 3.0 kcal·mol^{-1}. IM1b transforms into P1b ($C_3H_6O_6$, $HO_2CH_2OC(O)CH_2OOH$) via a concerted process of C_1-H_1 bond breaking in the Pent1a and C_1-C_3 and H_1-O_6 bonds forming with a barrier of 21.5 kcal·mol^{-1}. By comparing the barriers of R1a and R1b, it can be concluded that the –OOH insertion reaction is favored over the –CH insertion reaction. The high reaction barrier of R1b is attributed to the large bond dissociation energy (BDE) of C-H bond in the Pent1a. To further insight into the reaction mechanism of R1a, the natural bond orbital (NBO) analysis of the donor-accepter orbitals involved in the TS1a is performed using the M06-2X wave function. The possible donor-accepter interactions are estimated by using the second order perturbation theory. As illustrated in Fig. S4, the strong interactions are identified as the interaction of the lone pair orbital of O_6 atom and the antibonding orbital of O_4-H_4 bond, and the interaction of the lone pair orbital of O_4 atom and the antibonding orbital of C_3-O_5 bond.

Similarly, the addition reaction CH_2OO + P1a proceeds through the formation of the pre-reactive intermediates IM2a and IM2b in the entrance channel, which are stabilized by a hydrogen bond between the terminal oxygen atom of CH_2OO and the reacting hydrogen atom of P1a, and a van der Waals (vdW) interaction between the central carbon atom of CH_2OO and the carbonyl oxygen atom of P1a. The relative energies of IM2a and IM2b with respect to the separate reactants P1a and CH_2OO are -1.2 and 3.2 kcal·mol^{-1}, respectively, below the energies of the initial reactants $2CH_2OO$ and Pent1a are 41.6 and 37.2 kcal·mol^{-1}, respectively. Then they immediately transform into the respective products P2a and P2b through the –OOH and –CH insertion transition states TS2a and TS2b with the barriers of 10.1 and 21.6 kcal·mol^{-1}. This result again shows that the –OOH insertion reaction is favored kinetically. It deserves mentioning that the barrier of –OOH insertion reaction increases as the number of CH_2OO is increased. From the viewpoint of the geometrical parameters of TS2a and TS2b, the breaking O-H and C-H bonds are elongated by 14.8% and 20.6%, respectively, with respect to the equilibrium structures of IM2a and IM2b, while the forming C-O and C-C bond length are 2.013 and 2.264 Å, respectively. The result reveals that TS2a and TS2b are structurally reactant-like, which are consistent with the Hammond's hypothesis that the earlier transition states are generally exothermic (Hammond, 1955).

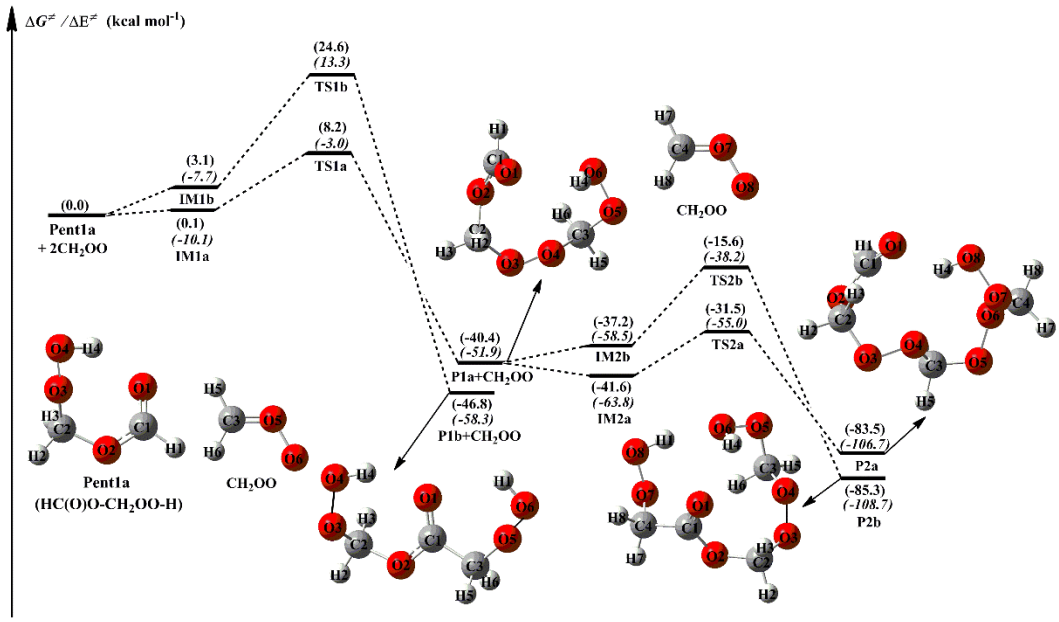

Figure 2. PES (ΔG and ΔE, in italics) for the $2CH_2OO$ + Pent1a reaction at the M06-2X/ma-TZVP//M06-2X/6-311+G(2df,2p) level of theory

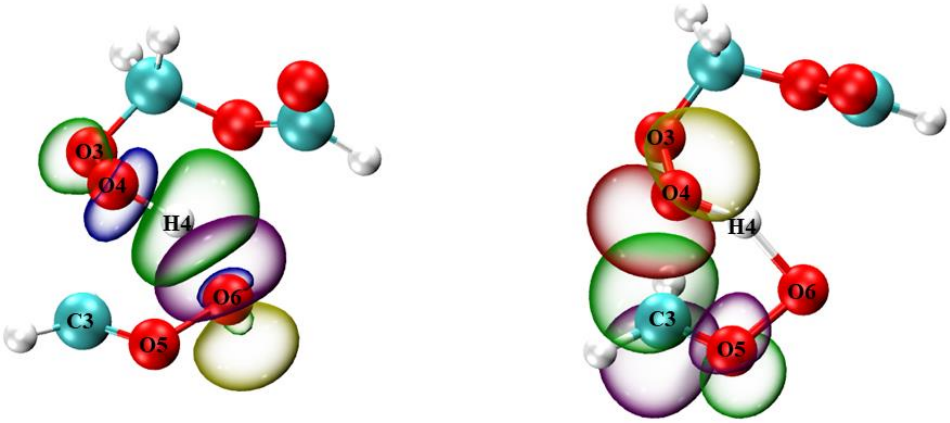

Figure S4. Natural bond orbital (NBO) analysis of the donor-acceptor orbitals involved in the TS1a

To further elucidate the effect of the number and location of methyl substituents on the reactivity of carbonyl oxides toward hydroperoxide esters, Pent1a (also called as HPMF) is selected as the model compound since it is the simplest hydroperoxide ester formed from the barrierless reaction of 1,4 O-H insertion of CH_2OO into HCOOH. As mentioned above, –OOH insertion reaction in the oligomerization reactions is the most favorable pathway. Therefore, this type of reaction is merely considered in the reactions of distinct SCIs with Pent1a. The corresponding PES is displayed in Fig. 6. As shown in Fig. 6, each pathway starts with the formation of a pre-reactive intermediate, and then it overcomes a modest barrier to reaction. The barrier of the reaction of CH_2OO with Pent1a is calculated to be 8.1 kcal·mol^{-1}, which is higher than that of the *anti*-CH_3CHOO + Pent1a reaction by 2.5 kcal·mol^{-1}. The reason of low barrier can be explained by the NPA atomic charges, as presented in Fig. S9. As seen in Fig. S9, the charges of the central carbon atom C_1 and the terminal oxygen atom O_1 of CH_2OO are 0.186e and -0.459e, respectively, indicating that CH_2OO is indeed a zwitterion. The C_1 atom charge becomes more positive (0.393e), while the O_1 atom charge becomes more negative (-0.497e) when a methyl substituent occurs at the *anti*-position. This result suggests that the *anti*-methyl substituent enhances the characteristic of carbonyl oxides zwitterion and reduces the reaction barriers. Compared with the barrier of the CH_2OO + Pent1a reaction, the barriers increase by about 3.0 kcal·mol^{-1} when a methyl group is introduced at the *syn*-position and dimethyl substituent. Although *syn*-methyl and dimethyl substituent promote the raise of carbonyl oxides zwitterion, the steric hindrance effect and intramolecular hydrogen bond are obviously dominant for *syn*-CH_3CHOO and $(CH_3)_2COO$, that are not thus conducive to the nucleophilic attack of hydroperoxide esters. It is worth noting that the exothermicity of distinct SCIs reactions with Pent1a obviously decreases as the number of methyl group is increased, and the

exothermicity of *anti*-methyl substituent is higher than that of *syn*-methyl substituent.

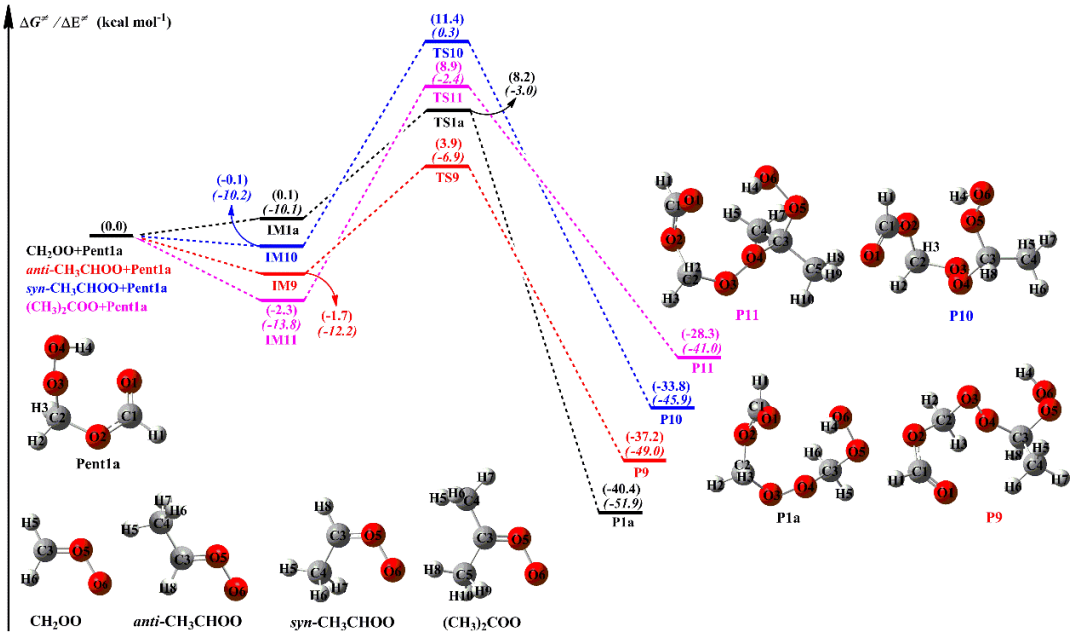

Figure 6. PES (Δ*G* and Δ*E*, in italics) for the distinct SCIs + Pent1a reactions at the M06-2X/ma-TZVP//M06-2X/6-311+G(2df,2p) level of theory

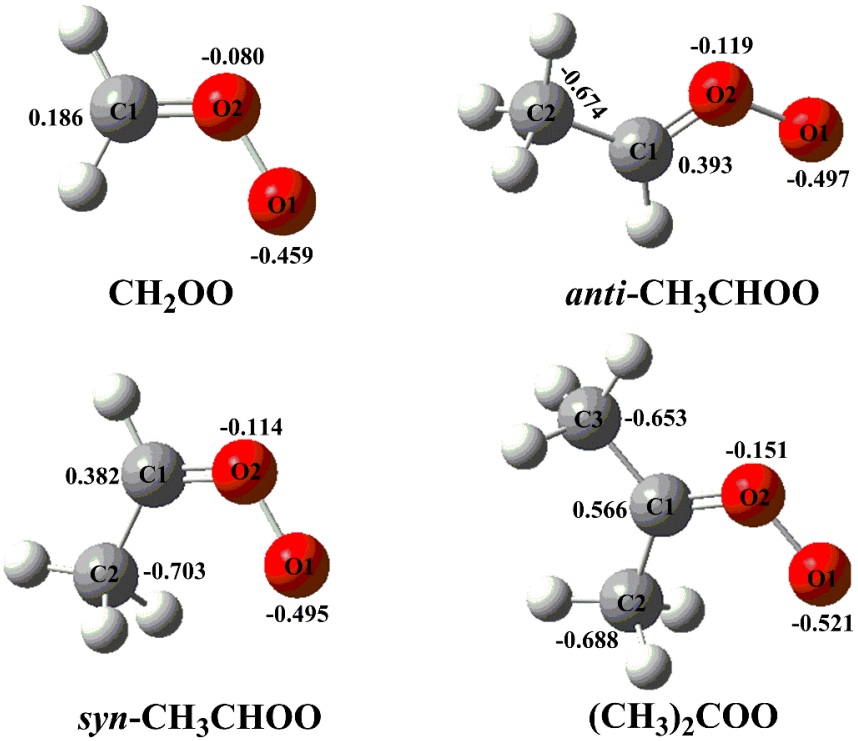

Figure S9 The NPA charges of different atoms in the distinct SCIs computed at the M06-2X/6-311+g(2df,2p) level of theory

Corresponding descriptions have been added in the page 15 line 388-398, page 16 line 399-438 and page 21 line 530-556 of the revised manuscript:

A schematic PES for the addition reaction 2CH_2OO + Pent1a is drawn in Fig. 2. As seen in

Fig. 2, the successive insertion of CH_2OO into Pent1a eventually leads to the formation of oligomers P2a and P2b composed of CH_2OO as the repeat unit. These oligomerization reactions are strongly exothermic and spontaneous (> 83 kcal·mol^{-1}), implying that they are feasible thermodynamically. The addition reaction $2CH_2OO$ + Pent1a initially proceeds through two possible pathways, namely (1) –OOH insertion reaction R1a, and (2) –CH insertion reaction R1b. For the –OOH insertion reaction R1a, the pre-reactive intermediate IM1a with a seven-membered ring structure is formed in the entrance channel, which is stabilized by the hydrogen bond interactions between the H_4 atom of Pent1a and the O_6 atom of CH_2OO ($D_{(O6\text{-}H4)}$ = 1.706 Å), and between the H_6 atom of CH_2OO and the O_3 atom of Pent1a ($D_{(O3\text{-}H6)}$ = 2.115 Å). Then IM1a converts into P1a ($C_3H_6O_6$, HC(O)O–$(CH_2OO)_2$–H) via a concerted process of O_4-H_4 bond breaking in the Pent1a and O_4-C_3 and H_4-O_6 bonds forming with a barrier of 8.1 kcal·mol^{-1}. For the –CH insertion reaction R1b, the pre-reactive intermediate IM1b with a seven-membered ring structure is formed in the entrance channel, which is stabilized by the van der Waals (vdW) interactions between the O_3 atom of Pent1a and the C_3 atom of CH_2OO ($D_{(O3\text{-}C3)}$ = 2.602 Å), and between the O_6 atom of CH_2OO and the C_1 atom of Pent1a ($D_{(O6\text{-}C1)}$ = 2.608 Å). Due to the absence of hydrogen bond in IM1b, the energy of IM1b is lower than that of IM1a by 3.0 kcal·mol^{-1}. IM1b transforms into P1b ($C_3H_6O_6$, $HO_2CH_2OC(O)CH_2OOH$) via a concerted process of C_1-H_1 bond breaking in the Pent1a and C_1-C_3 and H_1-O_6 bonds forming with a barrier of 21.5 kcal·mol^{-1}. By comparing the barriers of R1a and R1b, it can be concluded that the –OOH insertion reaction is favored over the –CH insertion reaction. The high reaction barrier of R1b is attributed to the large bond dissociation energy (BDE) of C-H bond in the Pent1a. To further insight into the reaction mechanism of R1a, the natural bond orbital (NBO) analysis of the donor-accepter orbitals involved in the TS1a is performed using the M06-2X wave function. The possible donor-accepter interactions are estimated by using the second order perturbation theory. As illustrated in Fig. S4, the strong interactions are identified as the interaction of the lone pair orbital of O_6 atom and the antibonding orbital of O_4-H_4 bond, and the interaction of the lone pair orbital of O_4 atom and the antibonding orbital of C_3-O_5 bond.

Similarly, the addition reaction CH_2OO + P1a proceeds through the formation of the pre-reactive intermediates IM2a and IM2b in the entrance channel, which are stabilized by a hydrogen bond between the terminal oxygen atom of CH_2OO and the reacting hydrogen atom of P1a, and a van der Waals (vdW) interaction between the central carbon atom of CH_2OO and the carbonyl

oxygen atom of P1a. The relative energies of IM2a and IM2b with respect to the separate reactants P1a and CH_2OO are -1.2 and 3.2 kcal·mol^{-1}, respectively, below the energies of the initial reactants $2CH_2OO$ and Pent1a are 41.6 and 37.2 kcal·mol^{-1}, respectively. Then they immediately transform into the respective products P2a and P2b through the –OOH and –CH insertion transition states TS2a and TS2b with the barriers of 10.1 and 21.6 kcal·mol^{-1}. This result again shows that the –OOH insertion reaction is favored kinetically. It deserves mentioning that the barrier of –OOH insertion reaction increases as the number of CH_2OO is increased. From the viewpoint of the geometrical parameters of TS2a and TS2b, the breaking O-H and C-H bonds are elongated by 14.8% and 20.6%, respectively, with respect to the equilibrium structures of IM2a and IM2b, while the forming C-O and C-C bond length are 2.013 and 2.264 Å, respectively. The result reveals that TS2a and TS2b are structurally reactant-like, which are consistent with the Hammond's hypothesis that the earlier transition states are generally exothermic (Hammond, 1955).

To further elucidate the effect of the number and location of methyl substituents on the reactivity of carbonyl oxides toward hydroperoxide esters, Pent1a (also called as HPMF) is selected as the model compound since it is the simplest hydroperoxide ester formed from the barrierless reaction of 1,4 O-H insertion of CH_2OO into HCOOH. As mentioned above, –OOH insertion reaction in the oligomerization reactions is the most favorable pathway. Therefore, this type of reaction is merely considered in the reactions of distinct SCIs with Pent1a. The corresponding PES and the optimized geometries of all stationary points are displayed in Figs. 6 and S8, respectively. As seen in Fig. 6, each pathway starts with the formation of a pre-reactive intermediate, and then it overcomes a modest barrier to reaction. The barrier of the reaction of CH_2OO with Pent1a is calculated to be 8.1 kcal·mol^{-1}, which is higher than that of the anti-CH_3CHOO + Pent1a reaction by 2.5 kcal·mol^{-1}. The reason of low barrier can be explained by the NPA atomic charges, as presented in Fig. S9. As seen in Fig. S9, the charges of the central carbon atom C_1 and the terminal oxygen atom O_1 of CH_2OO are 0.186e and -0.459e, respectively, indicating that CH_2OO is indeed a zwitterion. The C_1 atom charge becomes more positive (0.393e), while the O_1 atom charge becomes more negative (-0.497e) when a methyl substituent occurs at the anti-position. This result suggests that the anti-methyl substituent enhances the characteristic of carbonyl oxides zwitterion and reduces the reaction barriers. Compared with the barrier of the CH_2OO + Pent1a reaction, the barriers increase by about 3.0 kcal·mol^{-1} when a methyl group is introduced at the syn-position and

dimethyl substituent. Although syn-methyl and dimethyl substituent promote the raise of carbonyl oxides zwitterion, the steric hindrance effect and intramolecular hydrogen bond are obviously dominant for syn-CH_3CHOO and $(CH_3)_2COO$, that are not thus conducive to the nucleophilic attack of hydroperoxide esters. It is worth noting that the exothermicity of distinct SCIs reactions with Pent1a obviously decreases as the number of methyl group is increased, and the exothermicity of anti-methyl substituent is higher than that of syn-methyl substituent.

Reference

Barley, M. H., and McFiggans, G.: The critical assessment of vapour pressure estimation methods for use in modelling the formation of atmospheric organic aerosol, Atmos. Chem. Phys., 10, 749-767, https://doi.org/10.5194/acp-10-749-2010, 2010.

Canneaux, S., Bohr, F., and Henon, E.: KiSThelP: a program to predict thermodynamic properties and rate constants from quantum chemistry results, J. Comput. Chem., 35, 82-93, https://doi.org/10.1002/jcc.23470, 2013.

Chao, W., Hsieh, J. T., Chang, C. H., and Lin, J. J. M.: Direct kinetic measurement of the reaction of the simplest Criegee intermediate with water vapor, Science, 347, 751-754, https://doi.org/10.1126/science.1261549, 2015.

Chung, C. A., Su, J. W., and Lee, Y. P.: Detailed mechanism and kinetics of the reaction of Criegee intermediate CH_2OO with HCOOH investigated via infrared identification of conformers of hydroperoxymethyl formate and formic acid anhydride, Phys. Chem. Chem. Phys., 21, 21445-21455, https://doi.org/10.1039/c9cp04168k, 2019.

Donahue, N. M., Kroll, J. H., Pandis, S. N., and Robinson, A. L.: A two-dimensional volatility basis set – Part 2: Diagnostics of organic-aerosol evolution, Atmos. Chem. Phys., 12, 615-634, https://doi.org/10.5194/acp-12-615-2012, 2012.

Gilbert, R. G., and Smith, S. C.: Theory of unimolecular and recombination reactions; Blackwell Scientific: Carlton, Australia, 1990.

Glowacki, D. R., Liang, C. H., Morley, C., Pilling, M. J., and Robertson, S. H.: MESMER: an open-source master equation solver for multi-energy well reactions, J. Phys. Chem. A, 116, 9545-9560, https://doi.org/10.1021/jp3051033, 2012.

Hammond, G. S.: A correlation of reaction rates, J. Am. Chem. Soc., 77, 334-338, https://doi.org/10.1021/ja01607a027, 1955.

Huang, H. L., Chao, W., and Lin, J. J. M.: Kinetics of a Criegee intermediate that would survive high humidity and may oxidize atmospheric SO_2, Proc. Natl. Acad. Sci. U.S.A., 112, 10857-10862, https://doi.org/ 10.1073/pnas.1513149112, 2015.

Khan, M. A. H., Percival, C. J., Caravan, R. L., Taatjes, C. A., and Shallcross, D. E.: Criegee intermediates and their impacts on the troposphere, Environ. Sci.: Processes Impacts, 20, 437-453, https://doi.org/10.1039/C7EM00585G, 2018.

Long, B., Bao, J. L., and Truhlar, D. G.: Atmospheric chemistry of Criegee intermediates: unimolecular reactions and reactions with water, J. Am. Chem. Soc., 138, 14409-14422, https://doi.org/10.1021/jacs.6b08655, 2016.

Nannoolal, Y., Rarey, J., and Ramjugernatha, D.: Estimation of pure component properties Part 3. Estimation of the vapor pressure of non-electrolyte organic compounds via group contributions and group interactions, Fluid Phase Equilibria, 269, 117-133, https://doi.org/10.1016/j.fluid.2008.04.020, 2008.

Nannoolal, Y., Rarey, J., Ramjugernatha, D., and Cordesb, W.: Estimation of pure component properties Part 1. Estimation of the normal boiling point of non-electrolyte organic compounds via group contributions and group interactions, Fluid Phase Equilibria, 226, 45-63, https://doi.org/10.1016/j.fluid.2004.09.001, 2004.

Novelli, A., Hens, K., Ernest, C. T., Martinez, M., Nölscher, A. C., Sinha, V., Paasonen, P., Petäjä, T., Sipilä, M., Elste, T., Plass-Dülmer, C., Phillips, G. J., Kubistin, D., Williams, J., Vereecken, L., Lelieveld, J., and Harder, H.: Estimating the atmospheric concentration of Criegee

intermediates and their possible interference in a FAGE-LIF instrument, Atmos. Chem. Phys., 17, 7807-7826, https://doi.org/10.5194/acp-17-7807-2017, 2017.

O'Meara, S., Booth, A. M., Barley, M. H., Topping, D., and McFiggans, G.: An assessment of vapour pressure estimation methods, Phys. Chem. Chem. Phys., 16, 19453-19469, https://doi.org/10.1039/C4CP00857J, 2014.

Pankow, J. F., and Asher, W. E.: SIMPOL.1: a simple group contribution method for predicting vapor pressures and enthalpies of vaporization of multifunctional organic compounds, Atmos. Chem. Phys., 8, 2773-2796, https://doi.org/10.5194/acp-8-2773-2008, 2008.

Peltola, J., Seal, P., Inkilä, A., and Eskola, A.: Time-resolved, broadband UV-absorption spectrometry measurements of Criegee intermediate kinetics using a new photolytic precursor: unimolecular decomposition of CH_2OO and its reaction with formic acid, Phys. Chem. Chem. Phys., 22, 11797-11808, https://doi.org/10.1039/d0cp00302f, 2020.

Raghunath, P., Lee, Y. P., and Lin, M. C.: Computational chemical kinetics for the reaction of Criegee intermediate CH_2OO with HNO_3 and its catalytic conversion to OH and HCO, J. Phys. Chem. A, 121, 3871-3878, https://doi.org/10.1021/acs.jpca.7b02196, 2017.

Sipilä, M., Jokinen, T., Berndt, T., Richters, S., Makkonen, R., Donahue, N. M., Mauldin Iii, R. L., Kurtén, T., Paasonen, P., Sarnela, N., Ehn, M., Junninen, H., Rissanen, M. P., Thornton, J., Stratmann, F., Herrmann, H., Worsnop, D. R., Kulmala, M., Kerminen, V. M., and Petäjä, T.: Reactivity of stabilized Criegee intermediates (sCIs) from isoprene and monoterpene ozonolysis toward SO_2 and organic acids, Atmos. Chem. Phys., 14, 12143-12153, https://doi.org/10.5194/acp-14-12143-2014, 2014.

Taatjes, C. A., Welz, O., Eskola, A. J., Savee, J. D., Scheer, A. M., Shallcross, D. E., Rotavera, B., Lee, E. P. F., Dyke, J. M., Mok, D. K. W., Osborn, D. L., and Percival, C. J.: Direct measurements of conformer-dependent reactivity of the Criegee intermediate CH_3CHOO, Science, 340, 177-180, https://doi.org/10.1126/science.1234689, 2013.

Vereecken, L., Harder, H., and Novelli, A.: The reaction of Criegee intermediates with NO, RO_2, and SO_2, and their fate in the atmosphere, Phys. Chem. Chem. Phys., 14, 14682-14695, https://doi.org/10.1039/c2cp42300f, 2012.

Welz, O., Eskola, A. J., Sheps, L., Rotavera, B., Savee, J. D., Scheer, A. M., Osborn, D. L., Lowe, D., Booth, A. M., Xiao, P., Khan, M. A. H., Percival, C. J., Shallcross, D. E., and Taatjes, C. A.: Rate coefficients of C(1) and C(2) Criegee intermediate reactions with formic and acetic Acid near the collision limit: direct kinetics measurements and atmospheric implications, Angew. Chem. Int. Ed., 53, 4547-4550, https://doi.org/10.1002/anie.201400964, 2014.

Welz, O., Savee, J. D., Osborn, D. L., Vasu, S. S., Percival, C. J., Shallcross, D. E., and Taatjes, C. A.: Direct kinetic measurements of Criegee intermediate (CH_2OO) formed by reaction of CH_2I with O_2, Science, 335, 204-207, https://doi.org/10.1126/science.1213229, 2012.